

Compact Imaging Spectrometers using Acousto-Optic Tunable Filters

John J. Hillman,^a David A. Glenar,^b David M. Kuehn,^c Nancy J. Chanover,^d and William E. Blass^e

^a University of Maryland, Department of Astronomy, College Park, MD

^b NASA, Goddard Space Flight Center, Mail Code 693, Greenbelt, MD

^c Pittsburg State University, Department of Physics, Pittsburg, KS

^d New Mexico State University, Department of Astronomy, Los Cruces, NM

^e University of Tennessee, Department of Physics and Astronomy, Knoxville, TN

ABSTRACT

We describe planetary science observations made with the Goddard Space Flight Center, acousto-optic tunable filter (AOTF) cameras. This technology is a newly developed RF-tunable spectrophotometric imager. We describe four generations of AOTF camera designed, fabricated and demonstrated by the GSFC AOTF Camera Team over the decade of the 1990's. At each step making incremental steps toward the long-wavelength limit of the tellurium dioxide (TeO₂) AOTF cell material. TeO₂ is the most mature AOTF material and the best choice for operation at wavelengths in the 0.4-5.1 mm region. Because of several unique aspects of AOTF cameras, we briefly describe this technology in the introductory section. In Section 2 we describe our first camera which employed a Si CCD array. Adaptive optics observations of Jupiter and Saturn were made using this camera. Section 3 describes three versions of near-IR camera. It opens with a discussion of Venus observations made with our first near-IR camera employing Rockwell HgCdTe array technology. This camera had a 3.0-mm cutoff wavelength. Mars and Saturn were recently observed with our 3.8-mm camera. Our newest camera which we are completing this summer (2000) will extend the spectral range over 2.5-5.2 mm. We will discuss the new array performance and provide preliminary interpretations of some of these results.

1. INTRODUCTION

The theory of operation of the non-collinear AOTF has been reviewed by Glenar *et al.* 1994. The AOTF crystal is both birefringent and electro-optic. An RF acoustic wave is applied to the crystal. This sets up an internal phase grating by modulating the index of refraction due to a large elasto-optic coefficient. Each linear polarization state of the incoming light is diffracted into the opposite state and deflected upon exit from the crystal if its wavelength satisfies a specific momentum matching condition, $k_d = k_i \pm k_a$. Here k_d , k_i and k_a are the momentum vectors of the diffracted, incident and acoustic waves. To employ this filter in a camera concept, broadband, randomly polarized light is allowed to enter the AOTF crystal and the acousto-optic interaction causes a single wavelength to be divided into two polarization states which are symmetrically deflected at the output. These beams can be individually refocused into two monochromatic polarized images. Tuning is accomplished by changing the applied RF frequency to the ultrasonic transducer.

Optical throughput of the AOTF camera compares favorably with fixed multi-layer filters within its design tuning range and has a somewhat narrower bandpass than cooled CVF filters traditionally used at observatories. Acoustic energy is coupled into the crystal using a tin-bonded lithium niobate ultrasonic transducer. An RF tank circuit matches the impedance of the transducer to that of the RF source. Although TeO₂ is a usable acousto-optic material from 0.4 to 5.1 mm, the useful tuning range of a single device is generally limited to about one octave by the RF transducer matching circuit.

The in-band optical efficiency is defined by the single polarization efficiency, which is the fraction of input light in one polarization that is diffracted into the o' or e' output light at the passband peak. Typical single polarization efficiencies of AOTF cells used in our cameras are in the 70-80% range. Specific performance specifications can be found in the references cited for the specific camera of interest.

2. VISIBLE CAMERA

[Figure 1](#) shows the optical design of our visible AOTF camera. The foreoptics consist of a 5 mm x 6 mm input field stop and a field lens which reimages the telescope exit pupil onto a stop. The relay lenses reimage the field at 1:1 magnification near the AOTF input. A second field lens is placed here in order to image the pupil stop at infinity. This guarantees telecentricity, i.e. all of the light stays within a minimum divergence cone as it passes through the AOTF. This configuration allows the instrument to operate with telescopes as "fast" as $\sim f/12$ without loss of diffraction efficiency or spectral smearing. Note also that no physical stop is placed at the AOTF input where it can scatter or diffract light at extreme angles. Careful suppression of stray light is important in an AOTF instrument, because a very small fraction of the broadband undiffracted light can contaminate the narrow-band diffracted images, and make accurate flat fielding impossible. Upon exit from the AOTF, the orthogonally polarized beams are collimated and reimaged side-by-side on a rectangular CCD array. More complete details of this configuration can be found in Glenar *et al.* 1997.

This visible-wavelength camera has a spectral bandwidth of 25 cm^{-1} and a tuning range from about 0.5 to 1.0 μm , the Si CCD cutoff wavelength. Observations were made at the Starfire Optical Range 1.5-meter laser-beacon adaptive optics telescope facility. Observations were made of Jupiter and Saturn. The superior spectral resolution of the AOTF camera was exploited to image these objects both in and out of molecular absorption bands, allowing us to sound to different depths in their respective atmospheres. The Jupiter and some of the Saturn observations were made during the Comet Shoemaker-Levy 9 collisions in July 1994. Saturn (and Titan) was observed again in September 1995. The enhanced spatial resolution offered by the adaptive optics facility allowed us to observe cloud and storm activity in the atmospheres of Jupiter and Saturn that are not normally observable with conventional ground-based telescopes. Reviews of these observations can be found in Hillman *et al.* 1998(a), Hillman *et al.* 1998(b) and Chanover *et al.* 1999.

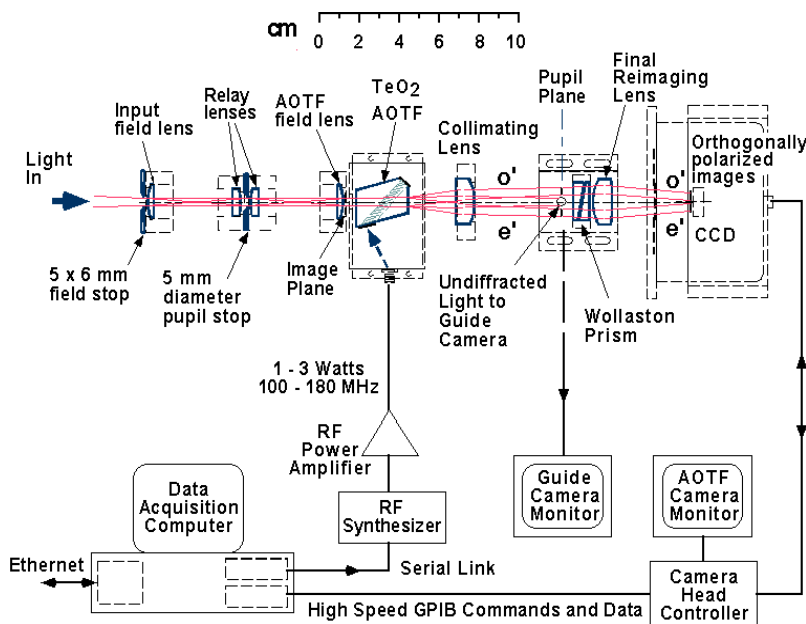


[Fig. 1](#)

3. NEAR-IR CAMERAS

[Figure 2](#) shows the near-IR camera components. They are mounted on a liquid nitrogen-cooled optical table housed in a IR Laboratories dewar. Although the optical design and layout have evolved over time, all our near-IR cameras use a similar dewar design. Mirror adjustments, for adjusting the focusing mirrors (H) and thermal switch control can be seen at the top of the dewar.

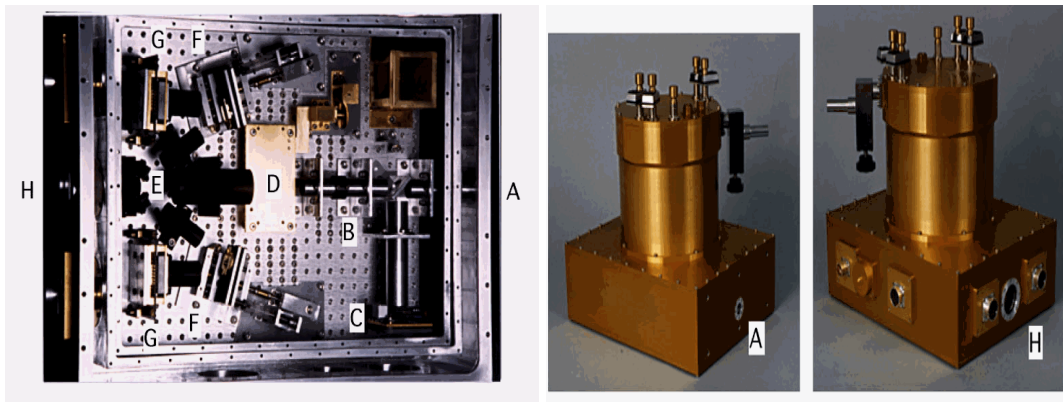


[Fig. 2](#)

3.1 PACE-1 3.0 mm CAMERA: Near-infrared imaging observations of the Venus nightside were made in 1996 at the Apache Point Observatory, Sunspot, NM. The AOTF camera had a measured spectral resolution of $1/D\lambda = 422$ at 2.3 mm. Chanover *et al.* 1998 reported on observations made at selected discrete wavelengths in the 2.3 mm spectral window in the Venus atmosphere. These data were sensitive to properties of the lower cloud deck of Venus. Zonal wind speeds near an altitude of 50 km were studied. These observations confirmed the approximately 5 day rotational period of the cloud features as well as observing contrast ratios of 20:1 corresponding to variation of optical depth of at least 8.

The focal plane array was a Rockwell Science Center device with a cutoff wavelength of 3.0 mm. Rockwell's approach for fabricating 256 x 256 format, NICMOS, 40 mm pixel FPA's was to hybridize PACE-1 HgCdTe detector arrays to CMOS switched FET readouts. The PACE-1 process for growing detector-quality HgCdTe on sapphire substrates is outlined in Gertner *et al.* 1985.

3.2 MBE PICNIC 3.8 mm CAMERA: This near-IR AOTF camera operates in the 1.7-3.6 micron region. This camera was used to obtain near-IR spectral image sets of Mars over the 1.6-3.6 micron region during the April 1999 opposition. A complete image set consisted of 280 images with a spectral full-width-half-maximum of 10 wavenumbers (fixed in frequency), 90 images in H-band (1.55-1.80 micron), 115 images in K-band (1.95-2.50 micron) and 75 images in L-band (2.90-3.70 micron). The short-wavelength limit is set by transmission of AOTF cell and long-wavelength limit is imposed by sensitivity of PICNIC, 256x256, HgCdTe array detector. These data are currently under analysis.

The PICNIC FPA was developed by Rockwell Science Center for the Jet Propulsion Lab *Pluto Integrated Camera Spectrometer (PICS)*. The PICNIC FPA is the latest device in the evolution of the NICMOS line of FPA's that have been designed and used by the astronomy community. Current manufacturing approach is based on using Molecular Beam Epitaxy (MBE) HgCdTe growth technology to fabricate planar p-on-n heterostructure photodiode arrays. This approach is outlined in Arias *et al.* 1994. These structures are grown on near lattice matched CdZnTe substrates to minimize the dislocation density in the HgCdTe epilayers.

3.3 MBE PICNIC 5.1 mm CAMERA : Our newest camera which we are completing this summer (2000) will extend the spectral range over 2.5-5.2 mm region. The 5.1 micron PICNIC array is controlled by a digital timing board developed by San Diego State University and marketed by Infrared Laboratories, Inc. It features a Motorola DSP56002 with a 24-bit data word, 16-bit address space and a Reduced Instruction Set Computer (RISC) architecture that executes most instructions in one clock cycle (40 ns). This unit controls a preamplifier unit that is attached to the dewar containing the infrared array and is thus in close proximity. For remote observatory operation the DSP is controlled via a fiber optic cable interfaced to an IBM-PC compatible (Dell Pentium II 450 MHz) running Windows 98, which can be at large distances from the detector. The DSP box also contains an RS-232 port through which an external device can be controlled. This port is used to control the RF frequency synthesizer, which is connected to the acousto-optic tunable filter.

In an effort to more efficiently collect images and to facilitate real-time data reduction and analysis, Interactive Data Language (IDL) from Research Systems, Inc. was used to develop the user interface. This programming language is in widespread use among astronomers and later versions of IDL feature "widgets", which are pre-defined graphically oriented programming objects. Since IDL is a very high-level language, it

has little ability to interface with custom hardware. IDL does have the ability to call external functions in a user-provided, dynamic link library (DLL). Using Microsoft's Visual C++ 6.0 Developer's Edition, two DLLs were constructed. One of these encapsulates the Infrared Laboratories DSP command structure, machine state, and communication protocol in a custom-defined object or "class". The other DLL provides a set of "wrapper" functions that follow IDL's prescribed definitions for calling external functions using a variable argument-passing scheme (e.g., the `argc` and `argv` variables of the C language).

The IDL user-interface for the infrared camera provides several imaging modes including the ability to obtain streaming video and single raw, differenced, and averaged frames. The user-interface also allows for the control and status monitoring of the RF outputs. Using this, the IDL program has the ability to take series of images and different RF frequencies (different AOTF passbands) and thus has can automatically obtain image cubes. The user-interface is "non-blocking", that is, it does not interfere with the interactive command prompt of IDL. This means that, without modifying the user-interface program's code, image processing, data reduction and analysis can be going performed while the program is running. Further, image arrays embedded within the user-interface can be directly accessed, so that other IDL applications can be run simultaneously to provide a data-reduction pipeline or diagnostic output, if needed.

Later this summer we will be conducting noise, gain and linearity measurements on the new array and completing the camera for the winter observing session.

REFERENCES

- Arias, J. M., J. G. Pasco, M. Zandian, J. Bajaj, L. J. Kozlowski, R. E. Dewames and W. E. Tennant, MBE HgCdTe flexible growth technology for the manufacturing of infrared photovoltaic detectors, *Proc. SPIE International Symp. on Optical Eng. In Aerospace Sensing, Orlando, FL* (1994).
- Chanover, N. J., D. A. Glenar and J. J. Hillman, Multispectral near-IR imaging of Venus night side cloud features, *J. Geophys. Res.* **103**, 31,335-31,348 (1998).
- Chanover, N. J., D. A. Glenar, J. J. Hillman, W. E. Blass, J. D. Drummond and R. Q. Fugate, Ground-based solar system astronomy using adaptive optics and acousto-optic tuning, *Adaptive Optics and Optical Interferometry, ASP Conference Series, B. Junor, ed.* **113**, xxx-xxx (1999).
- Gertner, E. R., W. E. Tennant, J. D. Blackwell and J. P. Rode, HgCdTe on sapphire – A new approach to infrared detector arrays, *Jou. Cryst. Growth*, **72**, 462 (1985).
- Glenar, D. A., J. J. Hillman, B. Saif and J. Bergstrahl, Acousto-optic imaging spectropolarimetry for remote sensing, *Applied Optics* **33**, 7,412-7,424 (1994).
- Glenar, D. A., J. J. Hillman, M. LeLouarn, R. Q. Fugate and J. D. Drummond, Multispectral imagery of Jupiter and Saturn using adaptive optics and acousto-optic tuning, *Pub. Astron. Soc. Pacific* **109**, 326-337 (1997).
- Hillman, J. J., D. A. Glenar, N. J. Chanover, and W. E. Blass, Acousto-optic cameras for tunable infrared spectral imaging of planetary atmospheres and surfaces, *Science with the NGST, ASP Conference Series, E. P. Smith and A. Koratkar, eds.* **133**, 257- 261 (1998)(a).
- Hillman, J. J., D. A. Glenar, G. Chin, N. J. Chanover, W. E. Blass, S. L. Mahan and M. Le Louarn, Hyperspectral AO observations of solarsyste objects, *Proc. ESO/OSA Topical Mtg., Astronomy with Adaptive Optics: Present Results and Future Programs, European Southern Observatory*, (1998) (b).